High-energy ARPES of Low-Dimensional Molybdenum Bronzes

J. D. Denlinger,[1] G.-H. Gweon,[1] J. W. Allen,[1] J. Marcus,[2] and C. Schlenker[2]

[1]Randall Laboratory, University of Michigan, Ann Arbor, Michigan 98109-1120, USA

[2]Laboratoire d'Etudes des Propiétés Electroniques des Solides, CNRS, BP166, 38042 Grenoble Cédex 9, France

INTRODUCTION

The molydenum bronzes, $K_{0.3}MoO_3$ (blue bronze) and $A_xMo_6O_{17}$, (A=Li, K,Na; purple bronze), are a class of charge density wave (CDW) materials that exhibit quasi-one dimensional (1D) and quasi-2D transport properties [1]. The Fermi surface (FS) topology for each bronze is of fundamental importance for the understanding of the Fermi surface nesting that gives rise to the CDW instability and hence gives motivation for performing angle-resolved photoelectron spectroscopy (ARPES) on these materials. In addition, Luttinger liquid behavior replaces normal Fermi-liquid behavior in the theory of one-dimensional interacting electron systems and such results might apply to 1D materials. For example, near-vanishing Fermi energy (E_F) spectral weight in angle-integrated photoemission measurements of the metallic phase of quasi-1D bronzes [2,3] could be explained in this way. However, care has to be taken to distinguish between this and other competing effects, such as strong 1D CDW fluctuations toward an E_F gap. Sufficiently resolved near-E_F ARPES spectra have the potential to signal such non-Fermi liquid behavior and to discriminate models.

Previous ARPES measurements of the molybdenum bronzes have been performed in the low photon energy regime of (15-40 eV) at other synchrotrons [4-8]. The purpose of additional ARPES measurements at the ALS is to explore the advantages and challenges of using (a) higher photon energies ($h\nu$>70 eV) and (b) automated angular-dependent measurements of small samples in a rotating-sample/fixed-detector geometry. In this abstract, the Fermi surface topologies of the quasi-1D Li purple bronze and quasi-2D Na purple bronze are illustrated and contrasted.

EXPERIMENT

Angle resolved measurements were performed at Beamline 7.0.1.2 with an experimental end-station originally designed for highly-automated angular and energy-dependent photoelectron diffraction [9]. The apparatus includes a 137-mm hemispherical spectrometer with 16-channel multi-detection and has proven very successful in the application of ARPES and Fermi-surface contour mapping to elemental metals and surfaces [10]. Samples were measured at room temperature with a total instrumental resolution of ≈80 meV and full angular acceptance of ≈1.4°.

The molybdenum bronzes present additional challenges compared to elemental substrates due to (a) the small sizes of available single crystals, (b) the small Brilluoin zone (BZ) resulting from a larger more complicated unit cell, and (c) susceptibility to beam damage. The molybdenum bronzes are grown by an electrolytic reduction technique [1] and are produced in sizes not larger than a few mm square. Clean surfaces are produced by *in situ* cleaving where the layered structure of the material improves the chances of large uniform surfaces of size similar to the sample itself. While the focused photon beam size (<100 μm) is much less than the sample size, the rotating sample geometry places tight restrictions on the alignment of the sample surface such that the incident beam does not wander off the sample or out of the analyzer analysis area. Even with careful attention to sample mounting, inherently different parts of the surface are measured for different sample angles. The BZ dimensions of the purple bronzes can be as small as 1.0 Å-1

which translates to only a ≈13° angular width of the BZ at the minimum photon energy available of 70 eV. Hence a 1.4° detector angular acceptance of 1.4° achieves a k-space resolution of ≈10% of the BZ width.

Beam damage to the molybdenum bronzes arises from creation of surface defects via photon-stimulated desorption of O atoms above the 4p→4d absorption threshold [11]. The effect is maximum around hν=50 eV and has the effect of suppressing Mo 4d spectral weight near E_F and creating a new defect emission feature at 2 eV binding energy. A typical molybdenum bronze valence spectra, shown in Fig. 1, consists of strong O 2p bands occupy 3-9 eV binding energy and weaker Mo 4d bands near E_F which are of primary interest. The progression of beam damage can be clearly monitored (dashed spectra in Fig. 1). The onset of spectral changes occurs with only a few minutes of dwell time at a single point on the sample using the intense fluxes from this undulator beamline. To minimize beam damage, an automated beam shutter was used while doing experiments, and the movement of the beam on the sample surface for different angles due to slight misalignments actually has a beneficial effect of reducing the beam exposure during automated angle scans. Measurement of many high resolution spectra, however, was problematic.

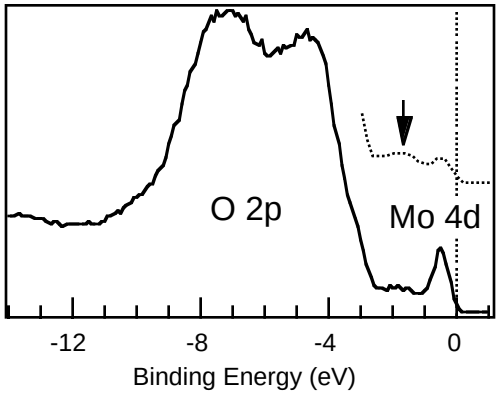

Figure 1. Li purple bronze valence spectra at hν=60 eV. The dashed spectra results after a few minutes of beam exposure.

Despite the severe inconveniences to being able to perform such experiments in this energy range or in this detection geometry, the assets of automation and multi-channel detection still allow some remarkable data to be collected.

$Li_{0.9}Mo_6O_{17}$

Li purple bronze has a large 1D anisoptropy in resistivity with an anomalous upturn in resistivity at 25 K (possibly a spin-density wave) and becomes superconducting at 2 K. Figure 2(a) shows a Fermi-edge angular intensity map at hν=70 eV for $Li_{0.9}Mo_6O_{17}$. The energy window used had a width of 0.4 eV centered at zero binding energy and the image shown is a result of 2-fold symmetrization of a 90° azimuthal sector of data. The symmetry axes of the Fermi-surface image was determined from the larger 360° raw data set. The azimuth alignment of the crystal was also checked *in situ* with Mo 3d x-ray photoelectron diffraction which exhibited a 3-fold symmetry arising from forward-scattering through near-neighbor oxygen atoms in MoO_6 octahedra structures that are linked in planar chains. Overplotted in Fig. 2(a) is the rectangular surface Brilluoin zone. The lack of horizontal crossings in the first BZ is due to surface homogeneity and/or beam damage. Figure 2(b) shows a vertical cut in k-space of the FE intensity obtained by polar scans at a series of photon energies (60-150 eV). The straight vertical lines of intensity verify the conservation of k-parallel at these E_F crossings.

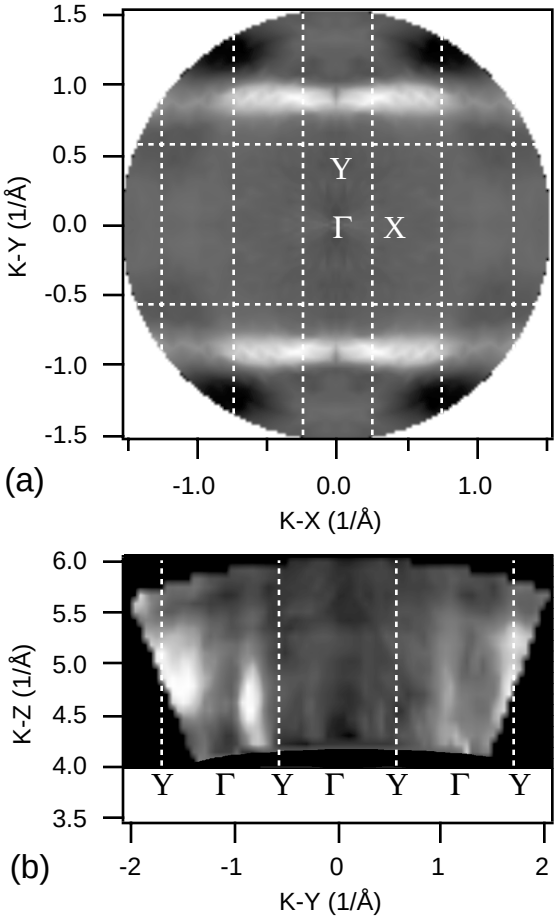

Figure 2. (a) Fermi-edge angular intensity map at hν=70 eV for quasi-1D $Li_{0.9}Mo_6O_{17}$, (b) Polar-photon FE-intensity map (hν=60-150 eV).

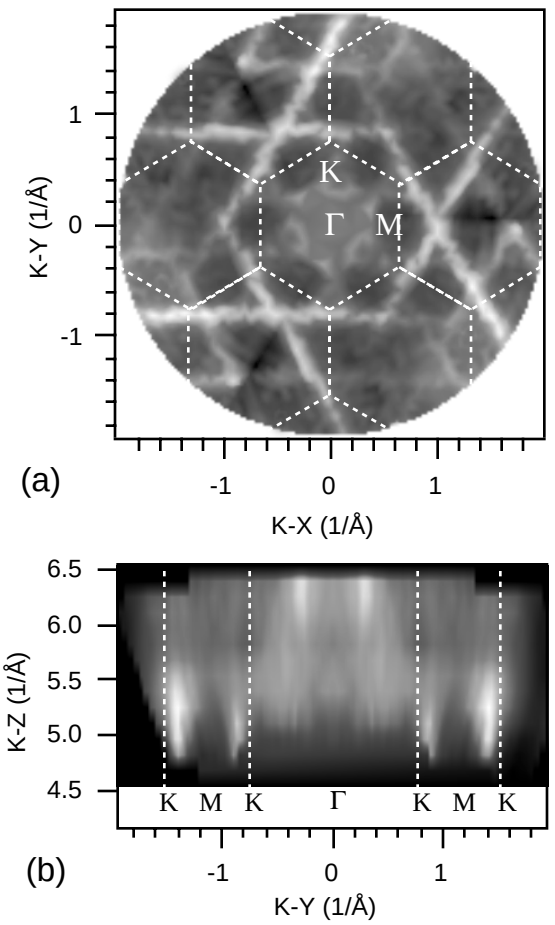

Figure 3. (a) Fermi-edge angular intensity map at hν=70 eV for quasi-2D $NaMo_6O_{17}$, (b) Polar-photon FE-intensity map (hν=70-160 eV).

$NaMo_6O_{17}$

Na purple bronze has a 2D anisotropy in resisitivity, undergoes a metal-metal CDW transition at about 80 K, and also becomes superconducting at 2 K. Similar to Fig. 2, angular and polar-photon E_F intensity maps for $NaMo_6O_{17}$ are shown in Figure 3. In contrast to the quasi-1D Li purple bronze, the k_x-k_y E_F intensity map for Na purple bronze shows a 3-fold pattern of criss-crossing parallel lines that form a 'Star of David' centered in each hexagonal BZ (dashed lines). This simple pattern, observed previously at low photon energy [7,8], arises because the electronic structure consists of weakly interacting quasi-1D chains oriented 120° to one another [12]. Again the intensity of the E_F crossings appear to be weaker in the first BZ and stronger in the second BZs. However, the k_y-k_z E_F map in Fig. 3(b) shows an energy dependence to this behavior with a clear reversal of E_F intensities in the first and second BZ at a higher photon energy of ≈150 eV.

Figure 4 illustrates the use of multi-channel detection to simultaneously measure a range of binding energies while performing an automated angular scan. At each point a snapshot of 16 energy channels is recorded with only ≈1 second dwell time instead of ≈30 sec required to acquire a full spectrum. Using a spectrometer pass energy of 12 eV, the spacing between detector channels is 0.1 eV and the total energy width of the snapshot is 1.6 eV. Figure 4 shows images recorded by 5 different channels corresponding to binding energies from 0.8 eV to 0 eV.

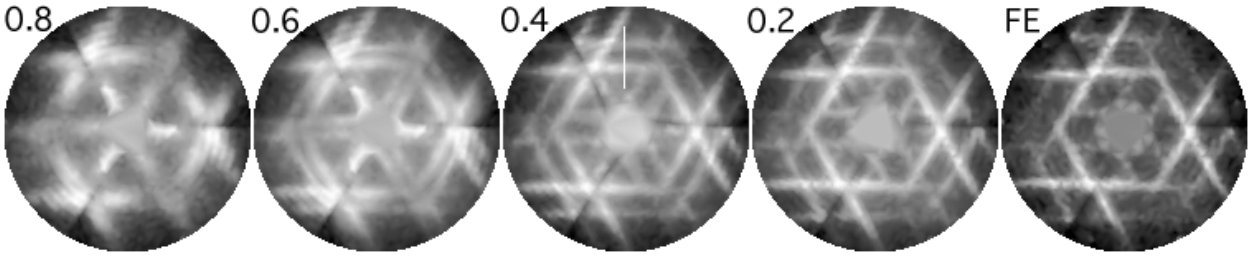

Figure 4. Constant binding-energy angular maps at hv=70 eV for $NaMo_6O_{17}$ simultaneously measured by the spectrometer 16-channel detection. Full 2π maps are obtained from 3-fold symmetrizing a 120° sector. The vertical line represents the polar angle range of Fig. 5.

This sequence of constant binding energy contours illustrates that the Fermi-surface is composed of *pairs* of lines linked by a dispersing band that disperses to ≈0.7 eV binding energy as shown in Fig. 5.

CONCLUSIONS

These results illustrate both the great potential and the great challenge of making such studies with this endstation.

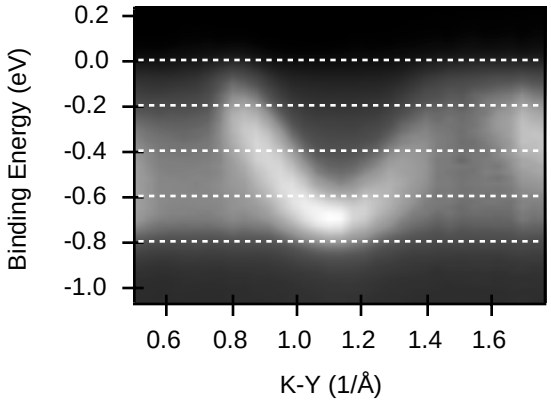

Figure 5. Image of Mo 4d valence spectra taken along K-M-K at hv=70 eV for $NaMo_6O_{17}$. Horizontal dashed lines illustrate the binding energies measured by multi-channel detection in Fig. 4.

REFERENCES

1. *Low Dimensional Electronic Properties of Molybdenum Bronzes and Oxides*, edited by C. Schlenker (Kluwer Academic Publishers, Dordrecht, 1989).
2. B. Dardel *et al*, Phys. Rev. Lett. **67**, 3144 (1991).
3. B. Dardel *et al*, Europhys. Lett. **19**, 525 (1992).
4. K. E. Smith, K. Breuer, M. Greenblatt, W. McCarroll, Phys. Rev. Lett. **70**, 3772 (1993).
5. K. Breuer *et al*, Phys. Rev. Lett. **76**, 3172 (1996).
6. M. Grioni *et al*, Physica Scripta **T66**, 172 (1996).
7. G.-H. Gweon *et al*, J. Phys. Condens. Matter **8**, 9923 (1996).
8. G.-H. Gweon *et al*, Phys. Rev. B **55**, 13353 (1997).
9. J. D. Denlinger *et al*, Rev. Sci. Instrum. **66**, 1342 (1995).
10. E. Rotenberg*et al*, Mater. Res. Soc. Symp. **437**, (1996); E. Rotenberg and S. D. Kevan, Phys. Rev. Lett. **80**, (1997), in press.
11. K. Breuer *et al*, Solid State Comm. **94**, 601 (1995).
12. M.-H. Whangbo, E. Canadell, P. Foury and J.-P. Pouget, Science **252**, 96 (1991).

This work was supported by the U.S. Dept. of Energy (DoE) under contract No. DE-FG02-90ER45416 and by the U.S. NSF under grant No. DMR-94-23741.

Principal Investigator: J. W. Allen, Department of Physics, University of Michigan. Email: jwallen@umich.edu. Telephone: 313-763-1150.